A comparison between different numerical models and experimental tests for the study of floating offshore wind turbines

Proceedings of the Thirty-third (2023) International Ocean and Polar Engineering Conference **www.isope.org**
Ottawa, Canada, June 19-23, 2023

ISBN 978-1-880653-80-7; ISSN 1098-6189

A comparison between different numerical models and experimental tests for the study of floating offshore wind turbines

Francesco Niosi, Oronzo Dell'Edera, Massimo Sirigu, Alberto Ghigo and Giovanni Bracco
Marine Offshore Renewable Energy Lab (MOREnergy Lab),
Department of Mechanical and Aerospace Engineering (DIMEAS),
Politecnico di Torino, Turin, Italy

ABSTRACT

The content of the present paper is the comparison between three different numerical models with the results of the experimental campaign conducted by the University of Plymouth, in the context of the 1st FOWT Comparative Study. Experimental tests were conducted to evaluate the hydrodynamic properties of a 1:70 scaled Volturn US semisubmersible floating platform, supporting a 15 MW offshore reference wind turbine coupled with the mooring system. This paper uses three different software with increasing numerical accuracy: MOST, Orcaflex, and STAR-CCM+. MOST is a numerical model developed by the Politecnico di Torino and implemented in a Matlab-Simscape environment; Orcaflex is a commercial software dedicated to offshore structure analysis, especially used for the design of mooring systems; STAR-CCM+ is commercial software for CFD analysis based on Unsteady Reynolds-Averaged Navier-Stokes equations (URANS). The tests considered for the validation of the experimental tests include free decay tests and focused wave tests. All the experiments are performed considering the 1:70 scaled Volturn US semisubmersible floating platform in its moored configuration. The results show how linear models, if properly calibrated, can provide more than satisfactory results with a low computational cost.

KEY WORDS: Offshore wind; floating offshore wind; 1st FOWT comparative study; numerical model; MOST; BEM theory; Orcaflex; CFD; STAR-CCM+; experimental tests.

INTRODUCTION

The interest in Floating Offshore Wind Turbines (FOWTs) is growing worldwide as the energy demand is increasing rapidly and the traditional energy sources are both environmentally and economically unsustainable. The floating technology would allow the exploitation of large sea areas at great distances from the coast, where the wind potential is greater and the seabed is too deep for bottom-fixed installations.
Today, many floating offshore wind foundations are available, some more consolidated, such as the spar-buoy or the semi-submersible, while others are still at an earlier level of design and experimentation (Ghigo et al. 2020). The first operative floating wind farm, Hywind Scotland was concluded in 2017, consisting of 5 spar-buoys supporting 6 MW devices for a nominal capacity of 30 MW. Currently, there are several floating wind farm projects, especially in the North Sea, along the Atlantic Ocean coasts and the Mediterranean Sea, but still in the preliminary stage. Among the main obstacles to the diffusion of floating offshore wind is the lack of public data, which can be used to verify and validate numerical models essential for assessing the performance of the various technologies. The most known open-source software is OpenFast (Jonkman et al. 2005), developed by National Renewable Energy Laboratories (NREL), which is considered the reference software for the simulation of floating offshore wind turbines. The main drawback of OpenFast is the poor readability of the source code, making it difficult to change the code and adapt to the user's different needs. As a result, numerous models have been developed over the last few years, as reported by Farraggiana et al. (2022), for different applications: to investigate the dynamic response of floating wind turbines (Liu et al. 2023), to increase the wind turbine productivity (Cottura et al. 2022), for the optimization of floating foundations (Ojo et al. 2022) and for the implementation of new control systems (Zhang et al. 2022).
To verify the reliability of the simulation results, the different codes are compared with the experimental tests proposed by the 1st FOWT Comparative Study referred to the experimental tests carried out at Plymouth University. Three different numerical models are used in this context: the first one is an in-house numerical MOST, an acronym that stands for Matlab for Offshore Wind Turbine Simulation Tool (Sirigu et al. 2022). The second tool is Orcaflex, a commercial software used for offshore structures applications developed by Orcina. Orcaflex is mainly used for sizing complex mooring systems of wave energy converters and floating offshore wind turbines (Ghigo et al. 2022). The third numerical model is developed in the STAR-CCM+ environment. The software computes the aerodynamics and hydrodynamics by solving the Navier-Stokes equations, while the mooring system is dynamically coupled to the CFD simulation and is modelled by Moordyn. While the first and the second tools have relatively low fidelity but require a small computational effort, the CFD model requires a high computational cost to have a high-fidelity result.
In the paper, a comparison between the three models will be carried out to

understand the pros and cons of each model and which condition MOST and Orcaflex fail concerning CFD simulations. Moreover, a comparison between the three numerical models and the experimental tests will be performed to assess experimental uncertainties, numerical modelling criticality, and numerical errors.

MOST MODEL

MOST is a code developed by MOREnergy lab, affiliated with the Politecnico di Torino. It is written in a Matlab-Simscape Multibody environment, which allows the user to analyze easily the multibody dynamics of the floating wind turbine. MOST was created to allow the user to implement different concepts like wave energy converters integrated with offshore wind platforms (Petrarca et al. 2022), flexible platforms, and platforms with multiple wind turbines. The theory implemented in MOST is described by Sirigut et al. (2022). In the last version of MOST, the code is expanded to simulate the six degrees of freedom. The hydrodynamics of the platform is evaluated using WEC-Sim, an open-source library code for Matlab developed by SANDIA and NREL (Ogden et al. 2021). It considers the hydrostatics, radiation damping, added mass, and excitation forces. Nemoh (Babarit et al. 2015) is used to evaluate the linear hydrodynamic coefficients. The radiation damping is evaluated using the convolution integral. The quadratic viscous forces are added externally to consider the nonlinear damping forces. The mooring forces are computed using the open-source code Moordyn (Hall et al. 2015), which is integrated with the Simscape model.

ORCAFLEX MODEL

Orcaflex solves the device dynamics in waves by numerically solving the time domain Cummins equation of motion (Cummins et al. 1962) accounting for both first-order and second-order hydrodynamics effects (Newman et al. 1979). To solve the time domain equation of motion, the hydrodynamic properties of the hull need to be defined through a Boundary Element Method (BEM) solver. OrcaWave, the BEM software developed by Orcina group, is used to obtain the hydrodynamic coefficients, such as added mass, damping coefficients and wave excitation forces, to be used in Orcaflex in the time domain simulations. Moreover, second-order hydrodynamic forces have been computed by using Newman's approximation instead of solving the full Quadratic Trasfer Function (QTF) problem (Newman et al. 2018). A mesh sensitivity analysis was performed to set the element size to obtain accurate hydrodynamic results (Niosi et al. 2022). Orcaflex solves the complete mooring system in the time domain. The mooring system is modelled using the analytic catenary equations which account for simple properties of a line such as its weight, buoyancy, and axial stiffness. The Orcaflex model is reported in Figure 1 and further explanations can be found in (Niosi et al. 2021).

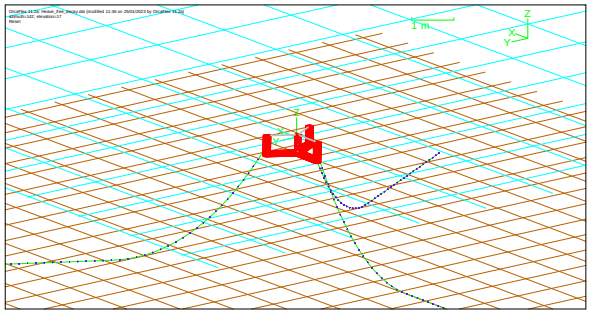

Fig. 1 Numerical model in forced heave oscillation.

These equations vary depending on whether the line is suspended above the seabed or laid down on the seabed. The line is divided into a series of segments, chosen to be 48 after a sensitivity analysis, and it is modelled accounting for its axial and torsional properties. The other properties (mass, weight, buoyancy, etc.) are all lumped into the nodes. A segment can be idealized as two co-axial telescoping rods connected by axial and torsional spring dampers. The forces acting on the mooring lines consider inertia forces, and all forces depend on previous states, such as drag forces. The dynamic model uses a formulation of Morison's equation for slender bodies with circular cross-sections.

HIGH FIDELITY MODEL

STAR-CCM+ is used to compute the dynamics of the body and to assess the hydrodynamic forces acting on the substructure. The inability of STAR-CCM+ to accurately compute the dynamics of the lines and their interaction with the seabed requires the use of other software or libraries to represent the mooring lines. For this reason, MoorDyn code is implemented as an external library. STAR-CCM+ uses the Dynamic Fluid Body Interaction (DFBI) (Tran et al. 2016) to calculate the platform kinematics at each time-step while MoorDyn calculates the tension along the mooring lines, as shown in Figure 2.

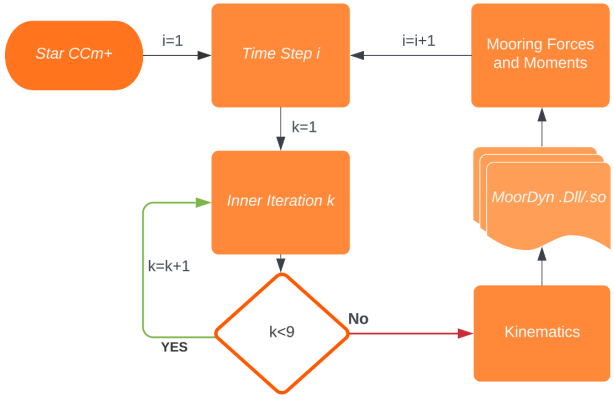

Fig. 2 Simulation Workflow.

The model developed in STAR-CCM+ is based on Unsteady Reynolds Averaged Navier-Stokes equations (URANS) with a turbulence model, as presented in previous work (Casalone et al. 2020 and Dell'Edera et al. 2022). The ideal parametric domain, which is thought to be the optimal compromise between computational cost and accuracy for the pure transport of waves, is used for all the tests described in this study. The numerical wave tank's geometry in 3 exhibits the following features:

- For the focused wave a reference wavelength has been chosen, which is equal to the wavelength of the greater harmonic of the focused wave.
- Two wavelengths in the y-direction; six wavelengths in the x waves propagation direction.
- The Water depth is set equal to the experimental wave tank depth.
- The bottom seafloor is a slip wall, the top of the numerical wave tank is a pressure outlet open to the atmosphere, and all the vertical walls in the wave tank, aside from the symmetry plane, are velocity inlets.
- For the Free Decay tests the same setup is employed aside from the dimension of the domain.

To ensure proper wave propagation, wave forcing is adopted at the velocity inlet (Siemens 2022). The forcing zone is a region where an analytic law is used to partially correct the momentum along the x and z axes as determined by the numerical resolution of the Navier-Stokes equations:

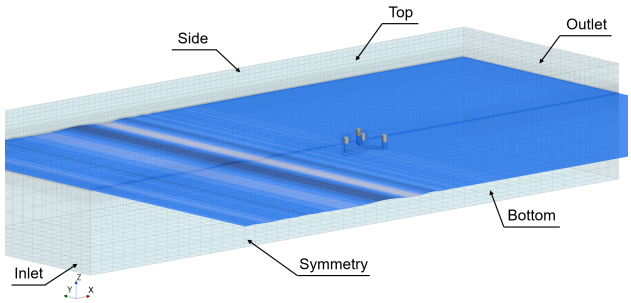

Fig. 3 Numerical wave tank in STAR-CCM+.

$$q_\phi = -\gamma\rho(\phi - \phi^*) \tag{1}$$

Where γ is the forcing coefficient, ρ is the fluid density, ϕ is the current solution, and ϕ' is the value towards which the solution is forced. Thanks to the work done by Peric et al. (2018,2019), it is now feasible to establish the ideal value of gamma for a particular regular wave to reduce wave reflection at the boundary. A forcing length equal to 2.5 λ is utilized for the domain's inlet and outlet and 1 λ for the side. The optimal value for γ was evaluated after considering the reflection contribution for each harmonic of the superposition wave. The mesh is crucial in ensuring proper wave propagation. In the model, two different regions are defined. The first one acts as the numerical wave tank. It is composed of trimmed cells and has several key characteristics to properly discretize the free surface, which are reported below: inferior

- AR_x is the ratio of the cells' length (x-direction) to their height (z-direction), and it equals 4.
- AR_y is the ratio of the width (y-direction) to the height (z-direction) of the cells, and it equals 16 far from the body and equals 4 for a distance of less than 1 wavelength.
- N is the number of cells in one wave reference height, which corresponds to the maximum wave height of the focused wave, which is equal to 32.
- Reduced computing costs are achieved using AMR, or adaptive mesh refinement (Wackers et al. 2017 and Warren et al. 1991). To achieve better discretization in the cells where gradients are stronger, this model permits the re-meshing of a small portion of the domain, close to the body and the free surface.

The second region is moving according to the body's kinematics. The mesh is constant and only the interface between the two regions changes during the simulations, thanks to the overset model described in detail in (Hadzic et al. 2006). For the mesh, polyhedral elements have been used while near the body a prism layer is used to correctly evaluate the viscus forces near the wall as suggested by (Deryugin et al. 2017).
The following models are employed to guarantee accurate modelling of the physics:

- 8 inner iterations per time step in a second-order temporal system. The time step was set to ensure that the maximum CFL at the air–water interface is between 0.1 and 0.2, as for values higher than 0.3 the wave's structure and period are no longer retained (Windt et al. 2018).
- The Convection term of the URANS is represented by a second-order upwind scheme since the first-order has enhanced damping as a result of numerical viscosity (Wang et al. 2018).
- The HRIC (High-Resolution Capturing Interface) system is used in conjunction with the VOF model to control multi-phase flows (Rhee 2005).
- A superposition of 1st-order Stokes waves is used to model the focused wave.
- The Dynamic Fluid Body Interaction (DFBI) model with 5 inner iterations is utilized to resolve the kinematics of the body (Tran et al. 2016).

The turbulence model used in the simulation is a novel approach implemented in STAR-CCM+, the Scale-Resolving Hybrid (SRH) turbulence model SRH. It is a variation of URANSand Deatached Eddy Simulations (DES) (Wilcox 2001), which enable the flow to be filtered both in time and space. URANS will never converge to a high-fidelity solution like LES/DNS, no matter how finely the mesh and time step are tuned. For DES/LES simulations, although the boundary layer can be modelled with decreased fidelity, the core flow still requires LES resolution and will not revert to RANS as the mesh and time step are coarsened. The SRH model detects which of the two is the limiting factor and modifies the eddy viscosity accordingly to always recover the best fidelity for a given mesh and time step if either the mesh or the time step is inadequately resolved. Using this novel approach the problem intrinsic to k-ϵ and k-ω of exponential growth of turbulent viscosity was prevented without using a limiter necessitated by classic turbulent models (Casalone et al. 2022, Larsen et al. 2018).

NUMERICAL MODELS SETTINGS

The following section describes the parameters used in the linear numerical models that require tuning due to the simplification of the problem's physics. In particular, it is shown a methodology to identify the linear and quadratic damping terms associated with the various degrees of freedom of the floating body. From the identification of the damping terms, the mooring system characteristics are identified. The damping is mainly influenced by two components: the viscous damping of the device, which in high-fidelity software is not defined as it is an intrinsic characteristic of the geometry of the body and the drag coefficients of the mooring lines. For linear models, an additional damping value is needed to account for the effect of the viscous forces. For this reason, three free decays without mooring were performed to determine the linear and quadratic damping of the substructure for each degree of freedom. Subsequently, the drag coefficients of the mooring lines were modified to match the damping evaluated in the free decay with mooring carried out within the experimental campaign. For the evaluation of the linear and quadratic term of the damping, the procedure described in (Fontana et al. 2020) has been used. The three models have identical mooring parameters. In such a way, the differences among them can be related only to hydrodynamic modelling. The outer diameter (OD) of the chains was calculated using the chain dry mass over the chain submerged mass relationship as reported in Equation 2.

$$w_s = 0.872 \cdot w_d \qquad w_s = w_d - \frac{\pi OD^2}{4} \cdot \rho_w$$

$$OD = \sqrt{\frac{4 \cdot w_d \cdot (1 - 0.872)}{\pi \cdot \rho_w}} \tag{2}$$

where w_s and w_d are respectively the submerged and dry masses over the length of the chain, ρ_w is the water density and OD is the outer diameter of the chain. The ratio $\frac{w_s}{w_s} = 0.872$ and the water density are reported by Ransley et al. (2022).
All the drag forces are evaluated by using the OD value. Particular attention must be paid to Orcaflex as on this software the diameters for calculating the forces are different from the OD by default. The stiffness

of the chains was calculated using the Orcina wizard based on the equivalent chain model. The mooring line added-mass coefficients are defined as suggested in the Orcaflex wizard. All the characteristics which are not detailed in (Ransley et al. 2022) of the mooring lines are reported in Table 1.

Table 1 Principal characteristics of mooring lines

Outer Diameter: OD (m)	0.00484
Normal Drag Coefficient: Cd_n	0.7225
Tangential Drag Coefficient: Cd_t	0.11
Normal Added Mass Coefficient: Ca_n	1
Tangential Added Mass Coefficient: Ca_t	0.5
Critical Damping Ratio: $(BA/-\zeta)\,(N\cdot s)$	-0.8

As anticipated before, the drag value of the chains has been calibrated according to the difference between the viscous damping values with and without mooring lines. As an example of the described procedure, Figure 4 shows the linear regression curve for the pitch free-decay without mooring, which allows the estimation of the linear and quadratic damping terms used for the calculation of the damping coefficients.

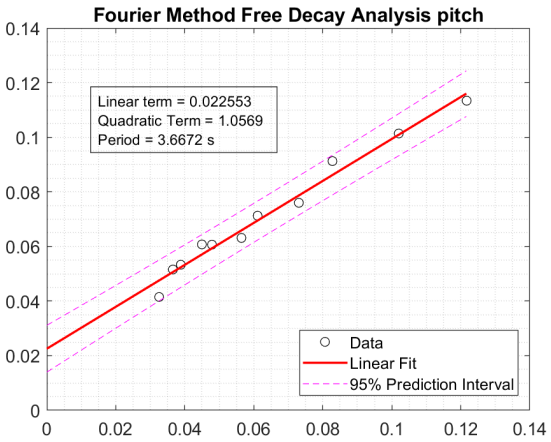

Fig. 4 CFD regression curve for Pitch Free Decay without mooring system

In Figure 5 is reported the same regression curve fitted on the time history of the pitch free-decay experimental data (with mooring lines).
By calculating the linear and quadratic damping coefficients (α,β), as detailed by Fontana et al. (2020), according to the Equation 3 and Equation 4, it is possible to calculate the vessel damping coefficients.

$$B_{vL} = 2\cdot\alpha\cdot(I_{ii} + A_{ii}(\omega_r)) \tag{3}$$

$$B_{vQ} = \beta\cdot(I_{ii} + A_{ii}(\omega_r)) \tag{4}$$

in which I_{ii} is the mass matrix term referred to the $i-DOF$, $A_{ii}(\omega_r)$ is the added mass term calculated by BEM software of the $i-DOF$ at the resonant frequency. α and β are the linear and quadratic terms of the regression curve. Once the viscous damping terms of the vessel are estimated, the drag coefficients of the mooring lines can be identified as the difference between the moored and the non-moored configurations. This procedure was performed for the pitch DOF and the drag coefficients of mooring lines have been set equal for all the other tests. In summary, the quadratic viscous damping terms for surge, heave, and pitch motions are reported in Table 2. Since the linear damping values are very small,

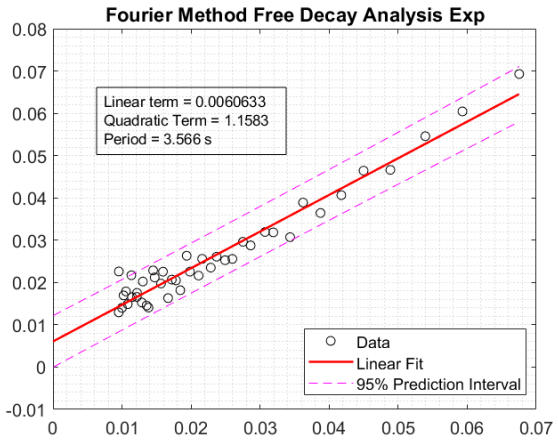

Fig. 5 Experimental regression curve for Pitch Free Decay with mooring system

their estimation can lead to numerical errors and since their influence with respect to quadratic terms can be neglected, they have been set as null values in the linear models. In addition to the quadratic damping value, the error inside the 95% confidence interval is reported in Table 2 and indicated as CI_{err}. In Table 2, $B_{Q_{NoMoor}}$ stands for quadratic damping with no mooring computed by CFD for the pitch motion and as a difference between experimental values and mooring drag for the surge and motions, B_Q stands for quadratic damping with no mooring,CI_{err} for error in the Confidence Interval for both moored and non-moored configurations, NP is the number of peaks analyzed in the Fourier Method and UM is the unit of measure.

Table 2 Principal characteristics of mooring lines

DOF	$B_{Q_{NoMoor}}$	CI_{err}	B_Q	CI_{err}	NP	UM
Surge	200	N.D.	214	±10%	7	$\frac{N}{(m/s)^2}$
Heave	1028	N.D.	1060	±7%	10	$\frac{N}{(m/s)^2}$
Pitch	35.7	±11%	39.2	±7%	25	$\frac{N}{(rad/s)^2}$

FREE DECAYS

The initial displacements given to the device during the execution of the numerical tests for the surge free decay were set equal to the values proposed by Ransley et al. (2022). In the same way, the initial displacements were also imposed for the pitch and heave tests. In the next section, the time histories of the main DOF associated with the performed test are reported. Furthermore, we compared the mooring line forces' time histories related to the forward mooring line and the aft-port mooring line at the fairleads. The aft-starboard mooring line was considered symmetric with respect to the aft-port mooring line. For surge, heave, and pitch free decays, the time history limit was set up to different values based on the period of oscillation.

Surge Free Decay

Table 3 displays the primary properties, namely the resonance period and the static equilibrium surge value.
A good agreement between numerical models and experimental tests can be noticed. In terms of resonance period, the experimental tests are smaller than the numerical models. This discrepancy may be associated with a minor shift in the centre of gravity or a slight mass variation. In

Table 3 Resonant Periods and Static mean for Surge FD

Value	Experimental	Orcaflex	MOST	STAR-CCM+
Td (s)	14.95	15.2	15.47	15.5
$Err.Td$	/	1.7%	3.5%	3.7%
Mean (m)	-0.0139	-0.0128	-0.0113	-0.0132

Table 4 Resonant Periods and Static mean for Heave FD

Value	Experimental	Orcaflex	MOST	STAR-CCM+
Td (s)	2.45	2.48	2.5	2.48
$Err.Td$	/	1.7%	2%	1.7%
Mean (m)	-0.021	-0.021	-0.023	-0.013

fact, as shown in Figure 6, a minor shift in the surge peaks occur. The periods of the numerical models differ slightly among them. This variance may be caused by an improper discretization of the CFD model, which necessitates a finer mesh size for this case.

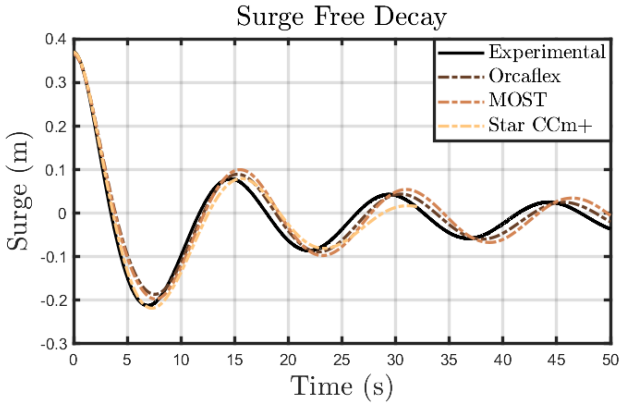

Fig. 6 Surge Free Decay Time History

Figure 7 illustrates the fairleads forces on the forward and the aft-port mooring lines. As can be seen, the values of the forces are fairly similar, indicating that the mooring system was well-modelled in all the numerical models.

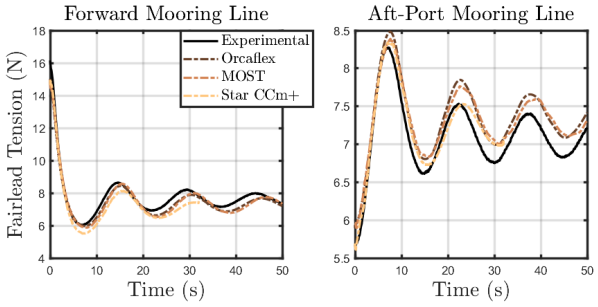

Fig. 7 Mooring Lines forces in Surge Free Decay

Heave Free Decay

In terms of free decay in heave, the kinematics and the forces appear to be consistent across the numerical models and the experimental tests. A special mention should be made concerning the heave static value computed through the high-fidelity model. An 8mm difference is noticed and it will be an object for further investigation (Table 4). All the following figures are reported accounting for this bias.

Concerning the first peak of the heave free-decay, only the CFD model can properly capture the device behaviour. This is due to a simplification of the damping models used in Orcaflex and MOST. In fact, the two linear models account only for linear and quadratic terms. The heave motion could require at least a third-order damping term component. The differences between the two damping approximations are significant only for large oscillations as can be seen in Figure 8.

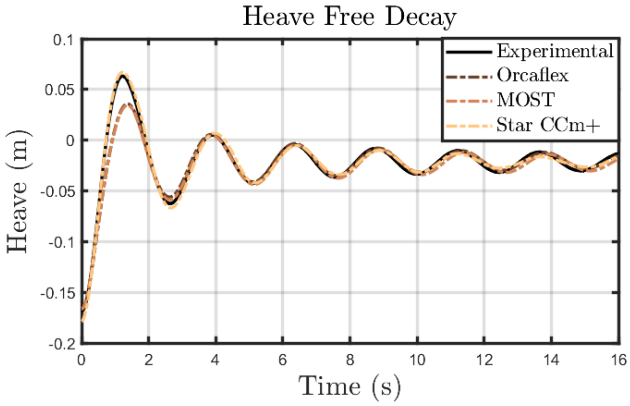

Fig. 8 Heave Free Decay Time History

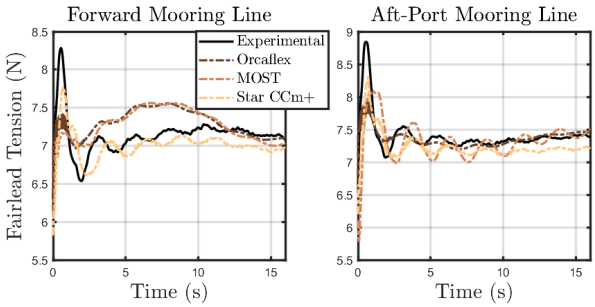

Fig. 9 Mooring Lines forces in Heave Free Decay

Pitch Free Decay

Table 5 displays the primary properties, namely the resonance period and the static equilibrium pitch value.

The resonance period in the various numerical models does not change considerably, although the period in the experimental tests does. This pattern can also be seen in Figure 10. This discrepancy may be caused by a slightly different inertia values. In fact, even minor changes might have a large impact on the resonance period.

There is also good agreement between numerical models and experimental tests regarding the forces acting on the mooring lines. Figure 11 shows the comparison between the numerical models and the experimental setup. It is noteworthy that there is a considerable difference between

Table 5 Resonant Periods and Static mean for Pitch FD

Value	Experimental	Orcaflex	MOST	STAR-CCM+
Td (s)	3.57	3.49	3.48	3.48
$Err.Td$	/	2.2%	2.5%	2.5%
Mean (deg)	-1.42	-1.38	-1.39	-1.24

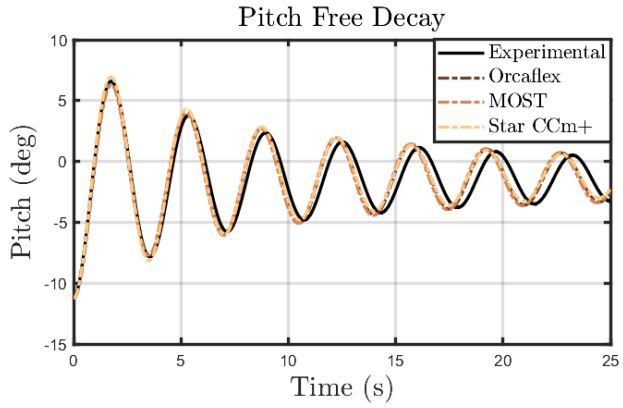

Fig. 10 Pitch Free Decay Time History

MOST and STAR-CCM+, which both use MoorDyn as a solver, especially for the aft-port mooring line. This is probably due to the coupling time step between the hydrodynamic solver and MoorDyn. In STAR-CCM+ a time step of 2 ms is used, while in MOST the time step is 10 ms.

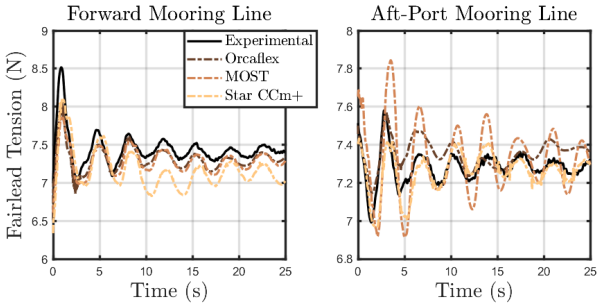

Fig. 11 Mooring Lines forces in Pitch Free Decay

FOCUSED WAVES

For the implementation of the wave profile in the numerical models, the following procedure was adopted: first, the wave elevation signal, acquired by the Wave Gauge n.6 (located at position $P(x,y) = (0,0)$) (Ransley et al. 2022) with no device, was filtered. Then, a signal was generated in such a way that the superposition of N-harmonic waves could replicate the desired time history. The number of components was chosen to reach a goodness of fit up to 99% in the interval of 45- 55 s, where the wave amplitude is maximum. An example of the reconstructed wave $FW1$ is reported in Figure 12.

It must be underlined that while in the linear models the implementation of the wave components is straightforward, in the CFD model is more complicated to reproduce an exact time. In fact, many simulation parameters influence the wave propagation. Because of that, before running the 3D CFD simulation a sensitivity study is performed on the mesh time step in a quasi-2D model, with a low computational cost.

The results obtained with the three numerical models are reported respectively for $FW1$ and $FW2$ in Figure 13 and Figure 14. In each Figure are plotted the surge, heave and pitch motion of the device and the wave elevation at $WG3$ position ($x = 0, y = -1.5$) (Ransley et al. 2022). It can be noticed that the wave elevation at $WG3$ is not reported for MOST because a further package must be implemented in the model to extrapolate the wave elevation for a given point. Furthermore, the Orcaflex wave elevation is computed considering the superposition of the radiated, diffracted and incident wave calculated through the potential formulation (Niosi et al. 2022). The high-fidelity model instead solves the RANS equations for wave propagation.

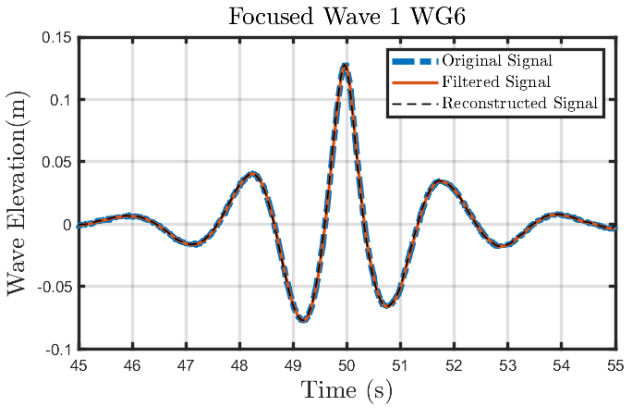

Fig. 12 Reconstruction of FW1

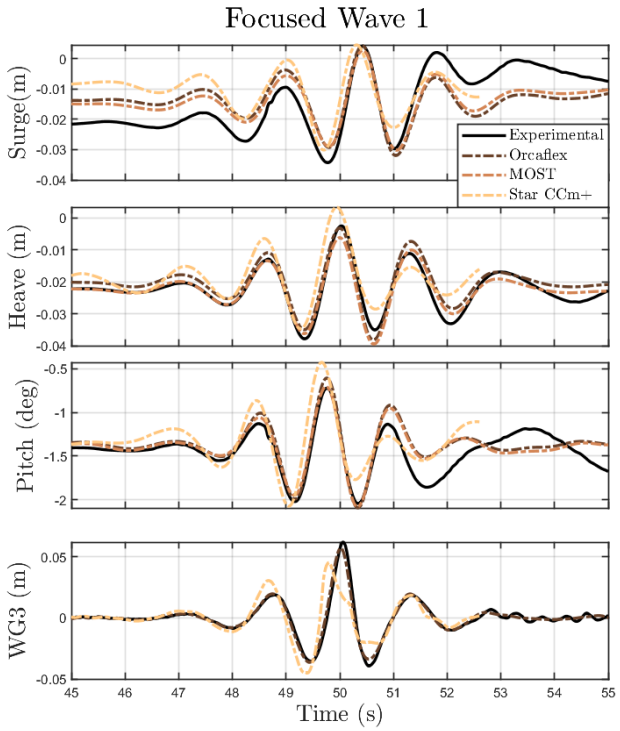

Fig. 13 FW1: Surge, Heave, Pitch and Wave Elevation at WG3

Despite the simplified hypotheses, the linear models better estimate the motion of the substructure. This is due to the error in the CFD model when generating the wave. In fact, referring to the wave elevation in the figures, it can be seen that the wave in the numerical tank also differs from the experimental data and it is less accurate than Orcaflex.

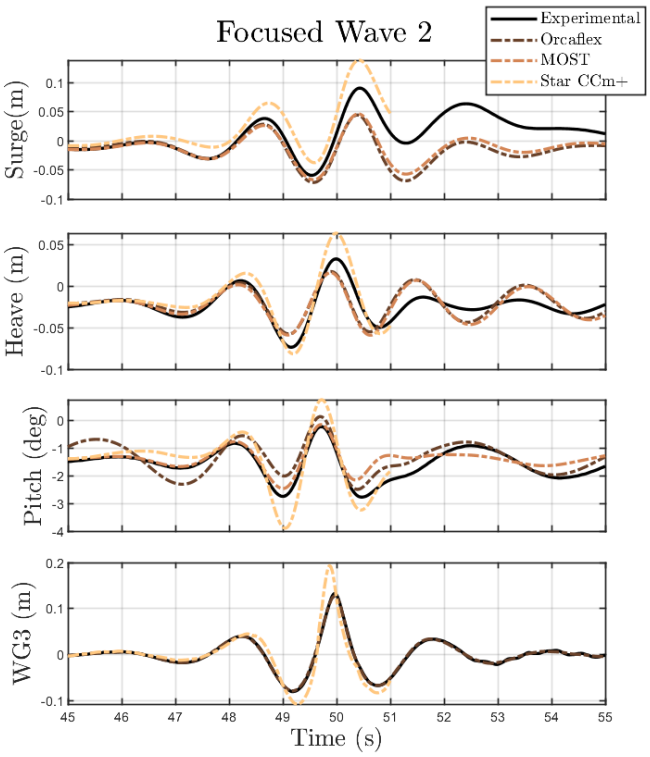

Fig. 14 FW2: Surge, Heave, Pitch and Wave Elevation at WG3

CONCLUSIONS AND DISCUSSION

In this article, the validation of the experimental tests carried out by the University of Plymouth and described by Ransley et al. (2022) was conducted to prove the reliability of the used numerical models. All the parameters specified in the dataset of the experimental campaign have been implemented in the numerical models, two of these are based on linear hydrodynamics theory and one on Navier-Stokes' equations. While Orcaflex and STAR-CCM+ are a commercial software, MOST is an open-source Matlab code, developed by the MOREnergy Lab research group. Linear models require a small computational cost but have lower accuracy, especially when the linearity hypothesis is not totally satisfied: however, their accuracy can be improved with an accurate determination of the non-linear hydrodynamic parameters. Thus, thanks to the free decay tests without mooring performed through the high-fidelity model, it was possible to identify the linear and quadratic viscous damping parameters to be included in the linear models. Furthermore, following this procedure, it was also possible to determine the drag coefficients of the mooring lines which, together with the other parameters of the mooring system described by Ransley et al. (2022), play a key role in the calculation of forces and moments and therefore also of the motions of the floating body. Barring small corrections that can lead to a slight improvement in the results, the comparison between the various numerical models and the experimental campaign was satisfactory, especially for the free-decay tests, where a good agreement between all the software was achieved. As far as the wave tests are concerned, the linear models prove to be reliable and are able to properly describe the dynamics. On the contrary, the high-fidelity model fails to faithfully reproduce the desired wave and so the kinematics of the substructure is different. Thus, the high-fidelity model requires more in-depth analysis for the setup when the wave propagation is critical and will be subject to further investigation. In this paper, we have seen how, in irregular waves, if linear models are properly tuned, they may lead to even more satisfactory results than a high-fidelity model requiring a remarkably lower computational cost but a higher modeling effort. An interesting possible future work, based on the results obtained in this work, is the identification of the experimentally measured parameters through an optimization algorithm aimed at improving the comparison between the numerical model and the experimental tests as experimental uncertainties may affect the system response. Specifically, the parameters that could be studied in this analysis are the inertia of the device, its center of mass, and the mooring lines length, since a very small variation of these parameters strongly affects the system dynamics.

REFERENCES

Babarit, A. and Delhommeau, G. (2015). "Theoretical and numerical aspects of the open source BEM solver NEMOH.", *In 11th European wave and tidal energy conference (EWTEC2015)..*

Casalone, P., Dell'Edera, O., Fenu, B., Giorgi, G., Sirigu, S. A. and Mattiazzo, G. (2020). "Unsteady RANS CFD simulations of Sailboat's hull and comparison with full-scale test. ", *Journal of Marine Science and Engineering, 8(6), 394*.

Casalone, P., dell'Edera, O., Fontana, M., Mattiazzo, G. and Battisti, B. (2022). "Solutions to wave damping over time in CFD RANS simulations due to exponential generation of numerical turbulence.", *In International Conference on Offshore Mechanics and Arctic Engineering (Vol. 85932, p. V008T09A084). American Society of Mechanical Engineers.*

Cottura, L., Caradonna, R., Novo, R., Ghigo, A., Bracco, G. and Mattiazzo, G. (2022). "Effect of pitching motion on production in a OFWT.", *Journal of Ocean Engineering and Marine Energy.*, 8(3), 319-330.

Cummins, W. E. (1962). "The impulse response function and ship motions.", *David Taylor Model Basin Washington DC*.

Dell'Edera, O., Casalone, P. and Giorgi, G. (2022, November). "Influence of the energy extraction system on the kinematics of a WEC: High-fidelity CFD with mooring and power extraction co-simulation. ", *In 2022 International Conference on Electrical, Computer, Communications and Mechatronics Engineering (ICECCME) (pp. 1-6). IEEE*.

Deryugin, Y. N., Sarazov, A. S. and Zhuchkov, R. N. (2017)."Features of overset meshes methodology on unstructed grids. ", *Matematicheskoe modelirovanie, 29(2), 106-118*.

Faraggiana, E., Giorgi, G., Sirigu, M., Ghigo, A., Bracco, G. and Mattiazzo, G. (2022). "A review of numerical modelling and optimisation of the floating support structure for offshore wind turbines.", *Journal of Ocean Engineering and Marine Energy.*, 8(3), 433-456.

Fontana, M., Casalone, P., Sirigu, S. A., Giorgi, G., Bracco, G. and Mattiazzo, G. (2020). "Viscous damping identification for a wave energy converter using CFD-URANS simulations.", *Journal of Marine Science and Engineering, 8(5), 355*.

Ghigo, A., Sirigu, S. A., Carapellese, F. and Bracco, G. (2022). "Design and Optimization of a Point Absorber for the Mediterranean Sea.", *In International Conference on Offshore Mechanics and Arctic Engineering, American Society of Mechanical Engineers.*, Vol. 85932, p. V008T09A088.

Ghigo, A., Cottura, L., Caradonna, R., Bracco, G. and Mattiazzo, G. (2020). "Platform optimization and cost analysis in a floating offshore wind farm.", *Journal of Marine Science and Engineering*, 8(11), 835.

Hadzic, H. (2006).“Development and application of finite volume method for the computation of flows around moving bodies on unstructured, overlapping grids. ”, *Technische Universität Hamburg*.

Hall, M. (2015). “MoorDyn user’s guide.”, *Department of Mechanical Engineering, University of Maine: Orono, ME, USA, 15.*.

Jonkman, J. M. and Buhl, M. L. (2005). “FAST user’s guide”, *Golden, CO, USA: National Renewable Energy Laboratory.*, (Vol. 365, p. 366).

Larsen, B. E. and Fuhrman, D. R. (2018). “On the overproduction of turbulence beneath surface waves in Reynolds-averaged Navier–Stokes models.”, *Journal of Fluid Mechanics, 853, 419-460*.

Liu, Z., Song, Y. and Chen, J. (2023). “Coupled rigid-flexible dynamics modeling and validations of floating offshore wind turbine.”, *Ocean Engineering.*, 267, 113200.

Newman, J. N. (1979). “The theory of ship motions. Advances in applied mechanics, 18, 221-283.

Newman, J. N. (2018). “Marine hydrodynamics ”, *The MIT press.*.(p. 448).

Niosi, F., Battisti, B. and Sirigu, S. A. (2022). “Influence of hydrodynamic interactions on the productivity of PeWEC wave energy converter array. ”, *In 2022 International Conference on Electrical, Computer, Communications and Mechatronics Engineering (ICECCME) (pp. 1-6). IEEE.*

Niosi, F., Parrinello, L., Paduano, B., Pasta, E., Carapellese, F. and Bracco, G. (2021). “On the influence of mooring in wave energy converters productivity: the pewec case. ”, *In 2022 In 2021 International Conference on Electrical, Computer, Communications and Mechatronics Engineering (ICECCME) (pp. 1-6). IEEE*.

Ogden, D., Ruehl, K., Yu, Y. H., Keester, A., Forbush, D., Leon, J. and Tom, N. (2022). “Review of WEC-Sim development and applications.”, *International Marine Energy Journal*, 5(NREL/JA-5700-83366).

Ojo, A., Collu, M. and Coraddu, A. (2022). “Multidisciplinary design analysis and optimization of floating offshore wind turbine substructures: A review.”, *Ocean Engineering.*, 266, 112727.

Perić, R. and Abdel-Maksoud, M. (2018).“Analytical prediction of reflection coefficients for wave absorbing layers in flow simulations of regular free-surface waves. ”, *Ocean Engineering, 147, 132-147*.

Peric, R. and Abdel-Maksoud, M. (2019).“Damping of non-linear and irregular long-crested free-surface waves using forcing zones. ”, *In 11th International Workshop on Ship and Marine Hydrodynamics (IWSH2019)*.

Petracca, E., Faraggiana, E., Ghigo, A., Sirigu, M., Bracco, G. and Mattiazzo, G. (2022). “Design and Techno-Economic Analysis of a Novel Hybrid Offshore Wind and Wave Energy System.”, *Energies.*, 15(8), 2739.

Ransley, E., Brown, S., Edwards, E., Tosdevin, T., Monk, K., Reynolds, A. and Hann, M. (2022). “Hydrodynamic response of a floating offshore wind turbine (1st FOWT Comparative Study Dataset).

Rhee, S. H., Makarov, B. P., Krishinan, H. and Ivanov, V. (2005). “Assessment of the volume of fluid method for free-surface wave flow.”, *Journal of marine science and technology, 10, 173-180*.

Siemens, P. L. M. (2022).“STAR-CCM+ User Guide. Siemens PLM Software Inc: Munich, Germany.

Sirigu, M., Faraggiana, E., Ghigo, A. and Bracco, G. (2022). “Development of MOST, a fast simulation model for optimisation of floating offshore wind turbines in Simscape Multibody.”, *In Journal of Physics: Conference Series.*, Vol. 2257, No. 1, p. 012003.

Tran, T. T. and Kim, D. H. (2016). “Fully coupled aero-hydrodynamic analysis of a semi-submersible FOWT using a dynamic fluid body interaction approach. ”, *Renewable energy, 92, 244-261*.

Turner, M., Peiró, J. and Moxey,G.(2016). “A Variational Framework for High-order Mesh Generation.”, *Procedia Engineering*, Vol. 163, pag. 340-352.

Wackers, J., Deng, G., Guilmineau, E., Leroyer, A., Queutey, P., Visonneau, M. and Liverani, A. (2017).“Can adaptive grid refinement produce grid-independent solutions for incompressible flows?. ”, *Journal of Computational Physics, 344, 364-380*.

WARREN, G., Anderson, W., THOMAS, J. and Krist, S. (1991).“Grid convergence for adaptive methods. ”, *In 10th Computational Fluid Dynamics Conference (p. 1592)*.

Wilcox, D. (2001). “Turbulence modeling-an overview.”, *In 39th Aerospace Sciences Meeting and Exhibit (p. 724)*.

Windt, C., Ringwood, J. V., Davidson, J., Ransley, E. J., Jakobsen, M. and Kramer, M. (2018, October).“Validation of a CFD-based numerical wave tank of the Wavestar WEC. ”, *In International Conference on Renewable Energies Offshore (p. 439). CRC Press*.

Zhang, H., Wang, H., Cai, X., Xie, J., Wang, Y. and Zhang, N. (2022). “Novel method for designing and optimising the floating platforms of offshore wind turbines.”, *Ocean Engineering.*, 266, 112781.